SIMULATION OF HELICOPTER NOISE IN MANEUVERING FLIGHT

Massimo Gennaretti¶, Jacopo Serafini, Marco Molica Colella, Giovanni Bernardini
Department of Engineering
Roma Tre University
Via della Vasca Navale 79
00146 Rome, Italy
¶m.gennaretti@uniroma3.it

Abstract

This paper deals with methodologies for evaluation of acoustic disturbance emitted by helicopter main rotors in unsteady maneuvers. The attention is focused on those techniques applied in minimum-noise, optimal trajectories search tools. Typically, noise optimization processes are based on noise estimations conceived as sequences of steady-state flight acoustic predictions, properly selected from dedicated databases. Introducing a multidisciplinary rotor solution procedure including accurate aerodynamic, aeroelastic and aeroacoustic prediction tools suited for unsteady maneuver analyses, this work presents an assessment of methods used for acoustic disturbance identification based on different characterization parameters for correlating unsteady flight conditions with steady-state flight radiated noise. Only the main rotor component is examined, although tail rotor contribution might be included, as well. The numerical investigation concerns a lightweight helicopter model in unsteady flight, and provides comparisons between noise predicted by the considered methods in terms of sound pressure levels on a hub-centered hemisphere rigidly connected to helicopter.

1 INTRODUCTION

Over the past decades, the prediction of aerodynamically generated noise has captured the attention of the rotorcraft research community and is nowadays an issue of primary interest in the design of modern helicopters. This is motivated by the need of following stricter noise standards for civil aircraft and by greater stealth required in military operations.

In the recent past, numerical tools suited to the determination of minimum-noise, optimal trajectories have been developed to alleviate the ground acoustic impact of helicopters (and, more generally, rotorcraft)[1,2]. These approaches often combine a flight simulation model, a near-field noise radiation model (acoustic source), a far-field noise propagation model and a geographic information system to let the optimization process consider orography and population density distribution of the interested area (in this context, as near-field noise it is intended the noise radiated in proximity of the rotorcraft, *i.e.,* at distances where atmospheric absorption, ground reflection and wind effects are still negligible while, differently from the far-field noise dominated by monopole-type radiation, monopole and dipole propagation are comparably relevant).

Usually, identified minimum noise trajectories correspond to unsteady maneuvers including turns, varying flight-path slope, accelerations and decelerations, which require acoustic source model update accordingly to change of flight conditions. During the optimization process, it is typically derived from an appropriate database of sound spectrum distributions over hemispheres surrounding the helicopter (the so-called noise hemispheres) obtained from rectilinear steady-state flights noise predictions[1,2,3]. However, the noise emitted during complex maneuvers may potentially be strongly affected by unsteady effects inducing inertial and aerodynamic loads variations, as well as by pitch, roll and yaw motions causing shifts in noise directivity[4]. Therefore, the selection of steady-state flight acoustic sources representing the approximation of maneuvering helicopter noise is a crucial issue in low-noise trajectory tools. Usually, this is accomplished in terms of a set of flight parameters chosen to characterize the noise source state. The most common criteria adopted to this scope consider as noise flight parameters either advance ratio and flight-path slope angle (Approach A, in the following), or advance ratio, rotor thrust coefficient, and rotor disk orientation with respect to relative wind (Approach B, in the following)[1,2,3].

The aim of this work is the analysis of the accuracy of such approaches in estimating the noise emitted by maneuvering helicopters through correlation with predictions provided by an acoustic tool suited for the

analysis of unsteady helicopter flights. The attention is focussed on main rotor component, but tail rotor contribution might be similarly included, as well. The evaluation of noise radiated by maneuvering rotorcraft is not an easy task, addressed by a restricted number of researchers in the last decades[5,4,6,7]. It requires the extension of the commonly-used steady flight solvers to non-periodic blade motion and loading, larger time scales of analysis, as well as the generalization of the numerical scheme applied to evaluate signal propagation time delay[7].

Here, the acoustic solver suited for maneuvering helicopters analyses is derived from application of the retarded-time Formulation 1A developed by Farassat[8] to integrate Ffowcs Williams and Hawkings's equation[9]. Further, observing that in maneuvering flights blade-vortex interaction (BVI) phenomena are often the main source of noise (see, for instance, ground approaches typically addressed by trajectory optimization processes), blade loads used in Formulation 1A are computed by free-wake aerodynamic/aeroelastic main rotor simulation tools capable of capturing with an appropriate level of a accuracy wake vorticity and wake-blade miss distance. In particular, main rotor loads and aeroelastic response are evaluated through a modal formulation applied to a nonlinear beam-like rotor blade model[10,11], coupled with a three-dimensional, boundary element method (BEM) for the solution of free-wake, potential flows[12,14]. Steady aeroelastic solutions are obtained by using a harmonic-balance approach[15], whereas fully unsteady solutions are evaluated through a time-marching procedure based on a Newmark-β integration scheme.

Considering a lightweight helicopter model in unsteady flight, numerical investigations are presented with the aim of assessing the accuracy of aeroacoustic simulations based on Approach A and Approach B, by comparison with those provided by the fully unsteady solver.

2 ASSESSMENT OF MANEUVER NOISE PREDICTION METHODS

Acoustic disturbance produced by helicopter flight is strongly dependent on the trajectory flown. Minimum-noise, optimal trajectory search processes (typically applied to approach flight-path identification) identify solutions consisting in a sequence of unsteady maneuvers, which include turns, variation of speed and flight-path slope angles (where BVI phenomena may play a crucial role). In these analyses, noise hemispheres considered as acoustic sources are derived from databases of steady, straight flight acoustic simulations. The approach is based on the assumption of approximating the radiated acoustic disturbance through a sequence of steady flight predictions corresponding to local operating conditions along the trajectory flown.

Commonly, the flight parameters used to characterize the steady flight acoustic noise source locally simulating the unsteady maneuver noise are either advance ratio, μ, and flight-path slope angle, γ, (Approach A), or μ, main rotor thrust coefficient, C_T, and tip-path plane orientation with respect to relative wind, α_{TPP} (Approach B)[1,2,3].

In order to assess the accuracy of the approximations introduced by Approaches A and B, for a given unsteady maneuver, acoustic predictions derived from their application are compared with those determined by the fully unsteady solution based on the general aeroacoustic formulation described in Section 3.

Specifically, considering an unsteady maneuver identified through a flight dynamics tool[16], the method of analysis consists in the following steps:

i for selected points along the trajectory, steady, rectilinear flights characterized by the flight parameters considered in Approach A and Approach B are trimmed;

ii a high-fidelity rotor aerodynamic-aeroelastic tool capable of capturing the complex blade-wake interaction phenomena affecting radiated noise (see Appendix A) is applied to determine blade pressure loads arising during Approach A and Approach B flights, as well as during the unsteady meneuver;

iii the acoustic disturbances generated by the unsteady maneuver and the two steady flights of Approach A and Approach B are evaluated through the aeroacoustic solver of Section 3, and the corresponding results are compared.

The flight dynamics tool applied in steady flight trimming and unsteady maneuver identification utilizes a low-fidelity main rotor model suited for this kind of problems[16]. This fact, combined with the observation that the prediction of rotor acoustic disturbance requires accurate evaluation of blade dynamics and aerodynamics (especially when BVI phenomena occur) motivates the introduction of high-fidelity, aeroelastic and aerodynamic solvers in the second step of the method of analysis.

3 AEROACOUSTIC SOLVER FOR ARBITRARY MANEUVERING FLIGHT

Noise radiated by rotor blades is evaluated through solution of the well-known Ffowcs Williams and Hawkings equation[9], which governs the propagation of

acoustic disturbances aerodynamically generated by moving bodies.

The boundary integral formulation developed by Farassat known as Formulation 1A[8] is a widely-used, computationally efficient way to determine solutions of the Ffowcs Williams and Hawkings equation, and is particularly suited for the problems examined here. When the velocity of the rotor blades is far from the transonic/supersonic range, it yields the aeroacoustic field as a superposition of two terms, both expressed by integrals evaluated over the actual blade surface, $S_{_B}$ [8]: the loading noise, $p'_{_L}$, related to the distribution of pressure over blade surfaces

$$
\begin{aligned}
(1)\quad 4\pi p'_L(\mathbf{x},t) = {} & \frac{1}{c_0}\int_{S_{_B}}\left[\frac{\dot{\tilde{p}}\,\mathbf{n}\cdot\hat{\mathbf{r}}+\tilde{p}\,\dot{\mathbf{n}}\cdot\hat{\mathbf{r}}}{r|1-M_r|^2}\right]_\tau \mathrm{d}S(\mathbf{y}) \\
& + \int_{S_{_B}}\left[\frac{\tilde{p}\,\mathbf{n}\cdot\hat{\mathbf{r}}-\tilde{p}\,\mathbf{M}\cdot\mathbf{n}}{r^2|1-M_r|^2}\right]_\tau \mathrm{d}S(\mathbf{y}) \\
& + \frac{1}{c_0}\int_{S_{_B}}\left[\frac{\tilde{p}\,\mathbf{n}\cdot\hat{\mathbf{r}}}{r^2|1-M_r|^3}\,r\dot{\mathbf{M}}\cdot\hat{\mathbf{r}}\right]_\tau \mathrm{d}S(\mathbf{y}) \\
& + \int_{S_{_B}}\left[\frac{\tilde{p}\,\mathbf{n}\cdot\hat{\mathbf{r}}}{r^2|1-M_r|^3}(M_r-M^2)\right]_\tau \mathrm{d}S(\mathbf{y})
\end{aligned}
$$

and the thickness noise, $p'_{_T}$, that depends on blade geometry and kinematics

$$
\begin{aligned}
(2)\quad 4\pi p'_T(\mathbf{x},t) = {} & \int_{S_{_B}}\left[\frac{\rho_0\dot{v}_n}{r|1-M_r|^2}\right]_\tau \mathrm{d}S(\mathbf{y}) \\
& + \int_{S_{_B}}\left[\frac{\rho_0 v_n\left(r\dot{\mathbf{M}}\cdot\hat{\mathbf{r}}+c_0M_r-c_0M^2\right)}{r^2|1-M_r|^3}\right]_\tau \mathrm{d}S(\mathbf{y})
\end{aligned}
$$

In the equation above, $\mathbf{r}$ denotes the distance between observer position, $\mathbf{x}$, and source position, $\mathbf{y}$, whereas $\hat{\mathbf{r}} = \mathbf{r}/r$ is the unit vector along the source-observer direction, with $r = |\mathbf{r}|$. In addition, c_0 and ρ_0 are the speed of sound and the density in the undisturbed medium, respectively, $\tilde{p} = (p - p_0)$ with p_0 representing the undisturbed medium pressure, $\mathbf{M} = \mathbf{v}_{_B}/c_0$ with $\mathbf{v}_{_B}$ denoting the body velocity, $M = \|\mathbf{M}\|$, $M_r = \mathbf{M}\cdot\hat{\mathbf{r}}$, and $v_n = \mathbf{v}_{_B}\cdot\mathbf{n}$, where $\mathbf{n}$ is the outward blade surface unit normal vector. Further, $\dot{v}_n$, $\dot{\mathbf{n}}$ and $\dot{\mathbf{M}}$ denote time derivatives of v_n, $\mathbf{n}$ and $\mathbf{M}$, observed in a frame of reference fixed with the undisturbed medium.

The integrals appearing in Eqs. (1) and (2) are evaluated by a zero-th order boundary element method: the blade surface is divided into quadrilateral panels, and the integrand functions multiplying kernel terms are assumed to be uniformly distributed within each panel, with values equal to those at the centroids. Notation $[...]_\tau$ indicates that these quantities are evaluated at the delayed source time, $\tau = t - \theta$, where θ is the time taken by the signal started from $\mathbf{y} \in S_{_B}$ to arrive in $\mathbf{x}$ at time t[8].

In problems dealing with weakly loaded rotors, thickness and loading noise are comparable. However, when strongly loaded rotors are examined, the thickness noise contribution tends to be negligible and the acoustic disturbance is dominated by the loading noise. Rotors in BVI conditions fall within this category of acoustic phenomena.

Commonly, applications of aeroacoustic formulations for helicopter rotor analysis consider steady, rectilinear, trimmed flights. In these operative conditions both kinematics and aerodynamics are periodic thus yielding, correspondingly, periodic integrand functions, periodic kernels and, for observers rigidly connected to a helicopter-fixed frame of reference, periodic delays as well (it is worth noting that the same periodicity occurs in coordinated turns).

Differently, during unsteady helicopter maneuvers kinematic and aerodynamic terms are non-periodic, thus increasing the complexity of the algorithms to be applied for implementing Eqs. (1) and (2). Time delays, θ, appearing in thickness and loading noise expressions are obtained as solutions of the following nonlinear equation

$$\|\mathbf{x}(t) - \mathbf{y}(t-\theta)\| = c_0\,\theta$$

and thus, the prediction of radiated noise requires the knowledge of the past time histories of blade pressure loads and vehicle and blade kinematics, for a time interval length depending on observer location. Indeed, time histories of center of mass trajectory and velocity, vehicle attitude and angular velocity are necessary data to evaluate instantaneous values of kernels and integral coefficients of the discretized versions of Eqs. (1) and (2), as well as the boundary conditions of the aerodynamic formulation applied to determine the non-periodic blade loads (see Appendix A).

4 NUMERICAL RESULTS

The numerical investigation on the assessment of noise prediction methods described in Section 2 concerns the unsteady flight of a lightweight helicopter model inspired by the BO105. The BO105 is a relatively small, multi-purpose helicopter with an empty mass of about 1200 kg and a maximum gross mass of 2300 kg. It has has a four-bladed, hingeless main rotor of 4.91 m radius, with blade pre-cone angle of 2.5° and rotor shaft tilted 3° forward. The two-bladed teetering tail rotor operates in pushing configuration; the tail surfaces are composed of a horizontal stabilizer and a vertical empennage, both fixed to the fuselage. The main geometrical, inertial and elastic characteristics of the helicopter model used here may be found in Ref. [17].

The unsteady flight considered consists in an ap-

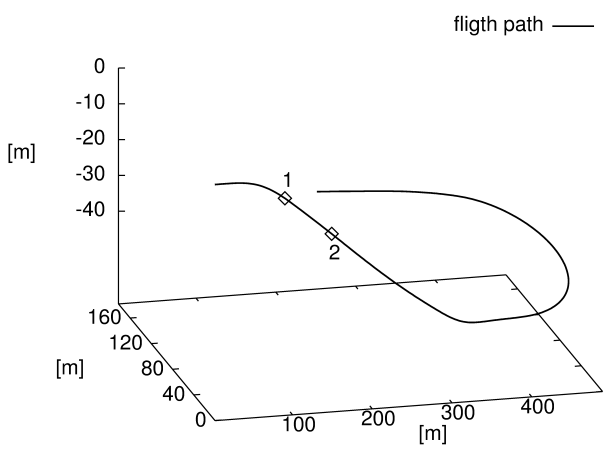

Figure 1: Flight trajectory.

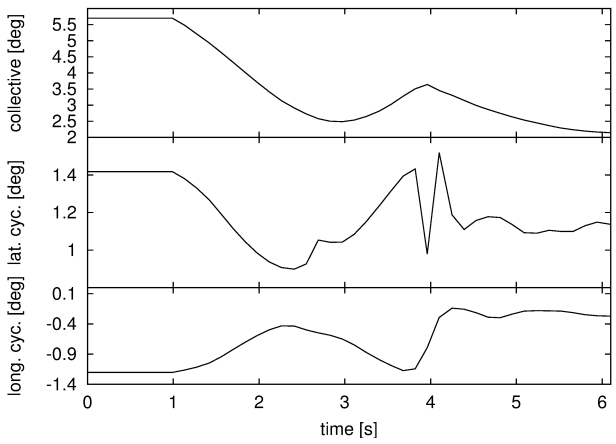

Figure 2: Blade controls in examined trajectory segment.

proach path starting from a level, steady rectilinear flight, followed by a straight, decelerating descent, a steady, banked, level turn, and finally a straight, uniform, level flight at very low speed[16] (see Fig. 1). The trajectory segment examined is the one flown during the first six seconds of the maneuver, with the attention focused on points 1 and 2 of Fig. 1. Point 1 is positioned at the transition from level to descent flight, while in point 2 the helicopter is in decelerated, rectilinear, descent flight.

It is worth noting that in point 1 the main difference between Approach A and B consists in C_T values, due to the significant load factor component arising along the rotor axis during the maneuver, while in point 2 inertial loads act along the tangent to the trajectory, thus altering rotor attitude with respect to wind, namely α_{TPP} (these inertial effects are taken into account in Approach B, but are hidden to Approach A). This is confirmed by Table 1 which shows trim blade pitch controls, $\theta_0, \theta_c, \theta_s$ and α_{TPP} at points 1 and 2, as determined by the application of Approach A and Approach B (positive α_{TPP} means backward rotor disk tilt with respect to relative wind). The time history of blade pitch controls concerning the unsteady flight are shown in Fig. 2.

Table 1: Blade pitch controls and rotor attitude

point/approach	θ_0	θ_c	θ_s	α_{TPP}
1/A	$4.05°$	$1.47°$	$-1.00°$	$6.37°$
1/B	$2.60°$	$1.14°$	$-0.69°$	$8.00°$
2/A	$3.80°$	$1.49°$	$-0.89°$	$7.91°$
2/B	$3.00°$	$1.40°$	$-0.89°$	$13.2°$

The aeroelastic response analyses have been performed considering three shape functions for flap, lead-lag and torsion deformations, whereas the aerodynamic BEM solver has been applied considering a blade surface discretization with 20 upper and lower chordwise panels, 24 spanwise panels, with time step of the time-marching solution corresponding to a blade azimuthal interval of $2\pi/216$ rad. Noise radiated by the rotor is presented in terms of overall sound pressure level (OASPL) and BVI sound pressure level (BVISPL), on a 50 m radius hemisphere fixed to the helicopter, with equatorial plane parallel to the cabin floor. Acoustic time signatures at specific points over the hemisphere are also examined.

4.1 Noise radiated at point 1

First, noise hemispheres evaluated at point 1 are examined.

Figures 4.1, 4 and 5 present the OASPL obtained through Approach A, Approach B and the fully unsteady aeroacoustic solver, respectively, for the helicopter advancing velocity directed towards the negative *x* axis of the plotted frame. Note that the OASPL from the unsteady simulation has been computed by applying an 1-rev-long Hanning window (centered at point 1 passage) to control the onset of leakage problems, along with a correction factor equal to 1.68 applied to the corresponding signal harmonics to compensate windowing effects on signal power. The comparison among these three noise hemispheres demonstrates that steady-state acoustics based on Approach B better captures unsteady effects, thus yielding results that are in closer, satisfactory correlation with those from fully unsteady simulations, both in terms of noise magnitude and directivity. Focusing on the area with higher noise level, an overestimation up to 5 db is provided by Approach A, whereas

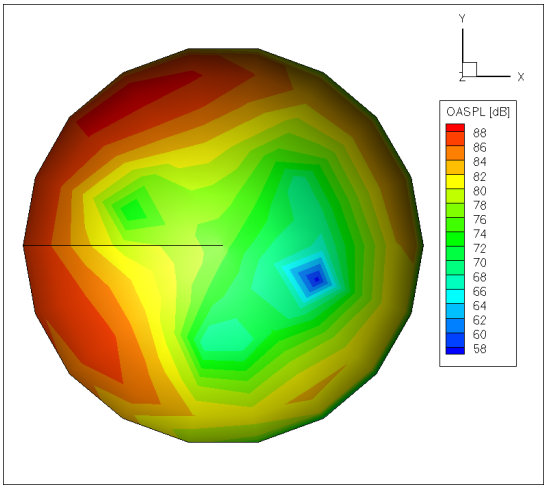

Figure 3: OASPL, Approach A, point 1.

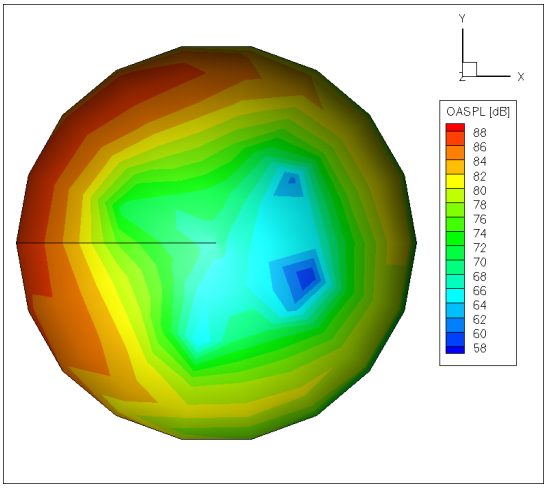

Figure 4: OASPL, Approach B, point 1.

a maximum discrepancy of about 1 db is observed in predictions by Approach B.

Next, the investigation is focused on the spectral content associated to blade-vortex interactions (BVIs) occurring at point 1 of the flown trajectory. These phenomena give rise to annoying acoustic effects that are of particular interest in the identification of optimal low-noise approach trajectories. Figures 6, 7 and 8 present BVISPL (that is derived from OASPL definition by neglecting noise harmonics below the 6-th blade-passage-frequency one) determined through the three prediction methods applied.

In this case, Approach A and Approach B provide results of similar quality. This is expected in that the differences between Approach A and B are related to inertial effects which, at point 1, are mostly reflected in axial load that, in turn, induces low-frequency ef-

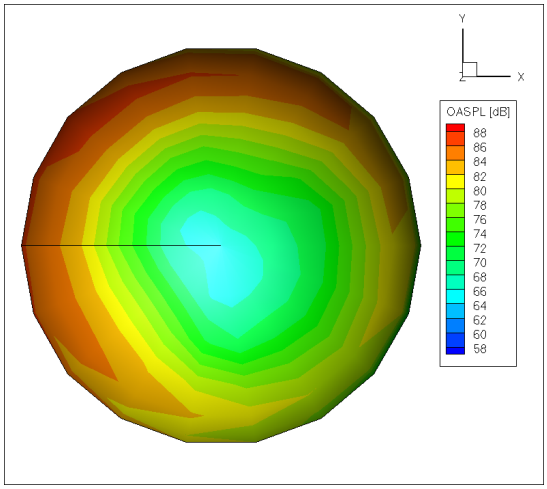

Figure 5: OASPL, unsteady simulation, point 1.

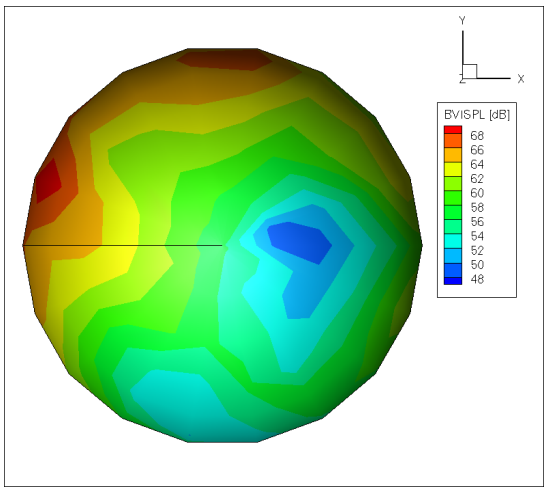

Figure 6: BVISPL, Approach A, point 1.

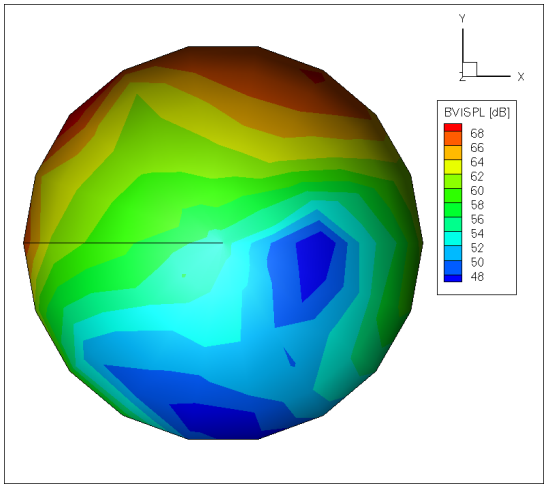

Figure 7: BVISPL, Approach B, point 1.

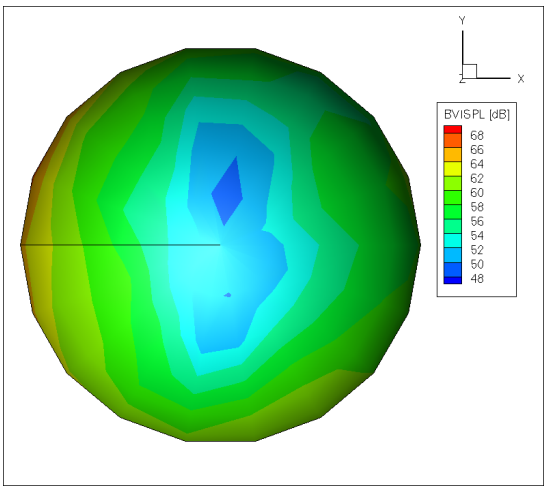

Figure 8: BVISPL, unsteady simulation, point 1.

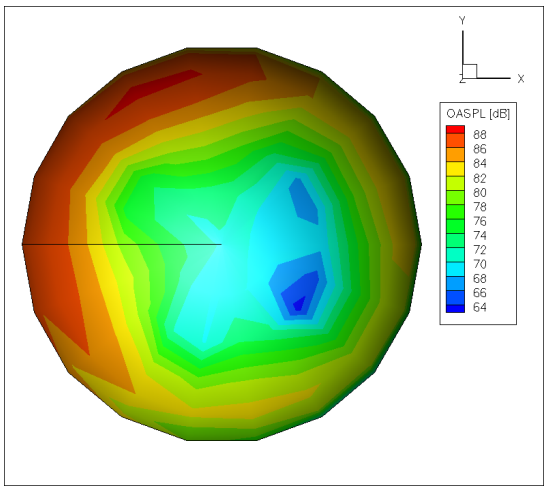

Figure 10: OASPL, Approach A, point 2.

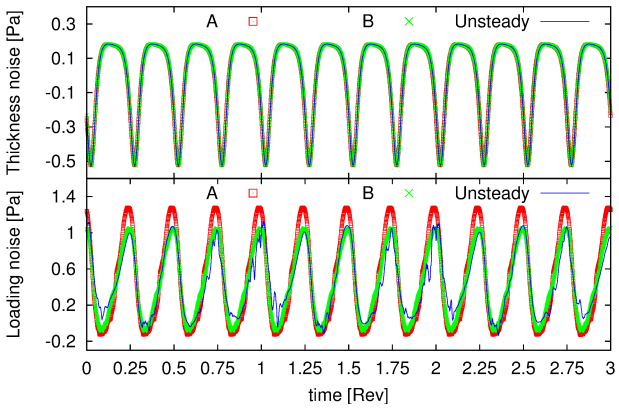

Figure 9: Thickness and loading noise at selected hemisphere microphone.

fects on disk loading. Both steady-state noise predictions show not negligible discrepancies with respect to those from the fully unsteady solver.

Finally, for an in-depth analysis of unsteady maneuver effects on radiated noise, the time signature at a specific microphone on the hemisphere is examined. For the selected microphone (having azimuth of $220°$ on equatorial plane and elevation of $-29°$), Fig. 9 presents thickness noise and loading noise predicted by the three approaches for a 3-second time interval centered at point 1. While thickness noise simulations are practically identical, loading noise is appreciably affected by unsteady maneuver effects, with predictions from Approach B closer to the fully unsteady solution.

4.2 Noise radiated at point 2

At this point of the trajectory the helicopter is in rectilinear, decelerated, descent flight. Inertial loads tangent to the trajectory, in combination with path slope and pitch attitude rate of change, cause remarkable variation of hub force along the vehicle longitudinal axis, of in-plane hub moments, and hence of rotor α_{TPP}, as shown in Table 1 (conversely, C_T is barely affected by inertial loads).

Figures 10, 11 and 12 present, respectively, the OASPL obtained at point 2 through Approach A, Approach B and the fully unsteady aeroacoustic solver. In this case, noise OASPL hemispheres predicted by Approach A and Approach B are of similar quality in terms of predicted noise magnitude and directivity, both showing appreciable discrepancies with respect to the fully unsteady results. The equivalent quality of steady-state OASPL predictions is expected because of the negligible influence of inertial loads on C_T, and hence on low-frequency noise.

Instead, the effect of inertial loads is highlighted by BVISPL analysis, which is remarkably affected by rotor attitude with respect to relative wind. Figures 13, 14 and 15, which present BVISPL determined through the three prediction methods applied, demonstrate that Approach B, taking into account the α_{TPP} generated by the unsteady maneuver, yields more accurate prediction for BVI noise peak than Approach A, and the two are in satisfactory agreement with those from the fully unsteady solver.

In particular, for most of the hemisphere area, Approach A overestimates BVI noise, although the corresponding α_{TPP} is lower than those considered in Approach B (see Table 1) during the unsteady maneuver. This is due to the very high value of α_{TPP} in the latter two cases that, combined with the disk load-

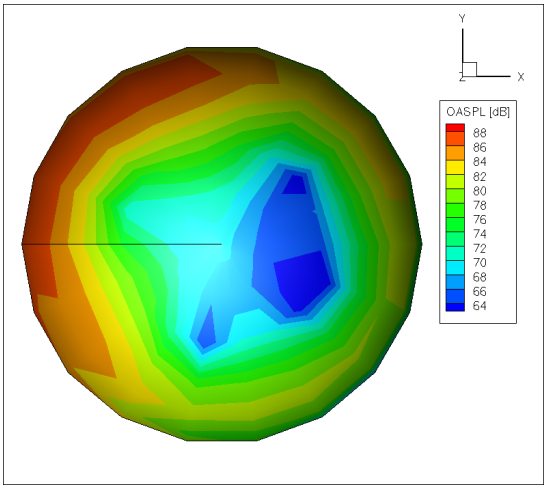

Figure 11: OASPL, Approach B, point 2.

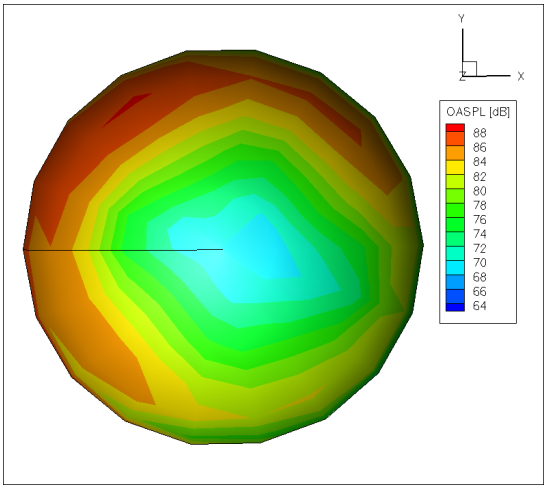

Figure 12: OASPL, unsteady simulation, point 2.

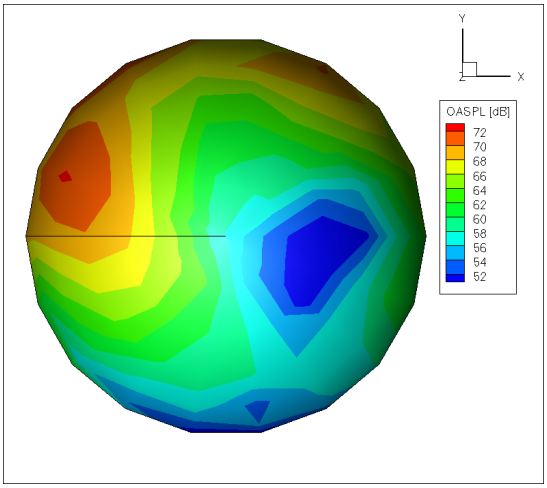

Figure 13: BVISPL, Approach A, point 2.

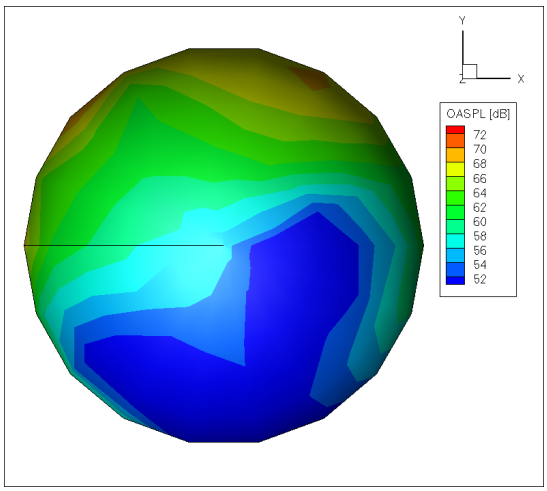

Figure 14: BVISPL, Approach B, point 2.

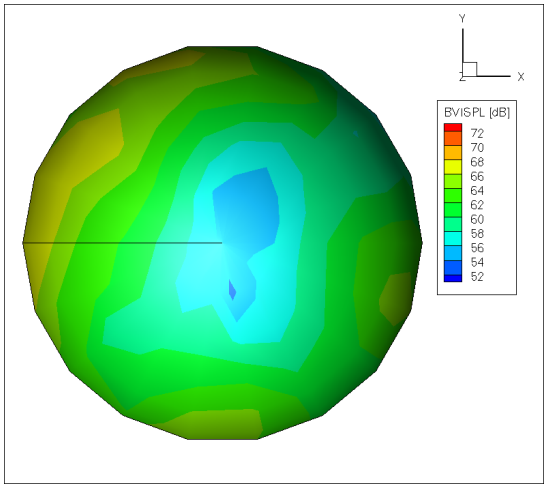

Figure 15: BVISPL, unsteady simulation, point 2.

ing, is such that the wake tends to move quicky far from the rotor, thus avoiding severe interactions with blades.

5 CONCLUSIONS

Considering an unsteady maneuver helicopter flight, noise predictions determined by a fully unsteady aeroacoustics solution approach tool introduced here, have been compared with those given by two steady-state noise simulation methods commonly applied in optimal-noise trajectory search tools (Approach A and Approach B, as defined above). Steady-state approaches are used in that avoid time-consuming, fully unsteady analyses that are unsuited for applications within optimization algorithms. The drawback is some inaccuracy introduced in the evaluation of radiated noise. The purpose of the presented numerical in-

vestigation has been the assessment of the quality of correlation between steady-state noise predictions and unsteady solutions. At the trajectory point where inertial loads mainly affect disk loading, Approach B yields OASPL predictions that satisfactorily correlates with unsteady solution, better than those by Approach A. However, high-frequency, BVI noise (barely affected by disk loading variations) is similarly captured by the two approaches, both showing a quite low level of accuracy, when compared with unsteady predictions. Conversely, at the trajectory point where inertial loads mainly affect rotor attitude with respect to relative wind, OASPL predictions (dominated by low-frequency noise) by Approach A and B are similar and show discrepancies with respect to fully unsteady simulation. Instead, BVISPL predicted by Approach B is more accurate than that by Approach A and is in fair correlation with unsteady solution. In the overall, the numerical investigation has demonstrated that: (i) steady-state approaches matching disk loading and rotor attitude occurring during an unsteady maneuver provide noise predictions of higher accuracy than those given by steady-state approaches matching only path slope; (ii) during an arbitrary maneuver, when inertial loads produce disk loading variation, low-frequency noise is mainly affected by unsteady effects, whereas when inertial loads affect rotor attitude, high-frequency, BVI noise changes appear; (iii) although some unsteady motion effects on radiated noise can be satisfactorily simulated by steady-state equivalent predictions, preliminary analyses presented here seem to demonstrate that they are not fully adequate to replace unsteady aeroacoustic solvers for predicting noise emitted by helicopters in arbitrary unsteady maneuvers.

ACKNOWLEDGMENTS

The research leading to these results has received funding from Project MANOEUVERS, financed by European Community's Clean Sky Joint Undertaking Programme under Grant Agreement N. 620068.
Further, the authors wish to thank Mr. Alessio Castorrini for his help in obtaining flight dynamics simulations used in this work.

REFERENCES

[1] D.A. Conner, J.A. Page, "A Tool for Low Noise Procedures Design and Community Noise Impact Assessment: The Rotorcraft Noise Model (RNM)," Proceedings of Heli Japan 2002, Tochigi, Japan, 2002.

[2] A. Le Duc, P. Spiegel, F. Guntzer, M. Kummer, J. Götz, "Modelling of Helicopter Noise in Arbitrary Maneuver Flight Using Aeroacoustic Database," Proceedings of the 9th Onera-DLR Aerospace Symposium (ODAS 2008), Chtillon, France, 2008.

[3] R.A. Morris, K.B. Venable, J. Lindsey, "Automated Design of Noise-Minimal, Safe Rotorcraft Trajectories," Proceedings of the 68th Annual Forum of the American Helicopter Society, Fort Worth, Texas, 2012.

[4] K.S. Brentner, H.E. Jones, "Noise Prediction for Maneuvering Rotorcraft," AIAA Paper 20002031, Proceedings of the 6th AIAA/CEAS Aeroacoustics Conference, Lahaina, Hawaii, 2000.

[5] R.D. Janakiram, H. Khan, "Prediction and Validation of Helicopter Descent Flyover Noise," Proceedings of the 56th Annual Forum of the American Helicopter Society, Virginia Beach, VA, May 2000.

[6] K.S. Brentner, G. Perez, G.A. Bres, H.E. Jones, "Toward a Better Understanding of Maneuvering Rotorcraft Noise," Proceedings of the 58th Annual Forum of the American Helicopter Society, Montréal, Canada, 2002.

[7] G.A. Bres, K.S. Brentner, G. Perez, H.E. Jones, "Maneuvering rotorcraft noise prediction," *Journal of Sound and Vibration*, Vol. 275, No. 3-5, pp. 719-738, 2004.

[8] F. Farassat, "Derivation of Formulations 1 and 1A of Farassat," NASA TM 214853, 2007.

[9] J.E. Ffowcs Williams, D.L. Hawkings, "Sound Generation by Turbulence and Surface in Arbitrary Motion," *Philosophical Transactions of the Royal Society*, London, Series A, Vol. 264, No. 1151, pp. 321-342, 1969.

[10] D.H. Hodges, E.H. Dowell, "Nonlinear Equation for the Elastic Bending and Torsion of Twisted nonuniform Rotor Blades," NASA TN D-7818, 1974.

[11] M. Gennaretti, M. Molica Colella, G. Bernardini, "Prediction of Tiltrotor Vibratory Loads with Inclusion of Wing-Proprotor Aerodynamic Interaction," *J. of Aircraft*, Vol. 47, No. 1, pp. 71-79, 2010.

[12] M. Gennaretti, G. Bernardini, "Novel Boundary Integral Formulation for Blade-Vortex Interaction Aerodynamics of Helicopter Rotors," *AIAA Journal*, Vol. 45, No. 6, pp. 1169-1176, 2007.

[13] G. Bernardini, J. Serafini, M. Molica Colella, M. Gennaretti, "Fully Coupled Structural-Unsteady Aerodynamics Modelling for Aeroelastic Response of Rotorcraft," Proceedings of 37th European Rotorcraft Forum, Gallarate, Italy, 2011.

[14] G. Bernardini, J. Serafini, M. Molica Colella, M. Gennaretti, "Analysis of a Structural-Aerodynamic Fully-Coupled Formulation for Aeroelastic Response of Rotorcraft," *Aerospace Science and Technology*, Vol. 29, No. 1, pp. 175-184, 2013.

[15] M. Gennaretti, G. Bernardini, "Aeroelastic Response of Helicopter Rotors Using a 3-D Unsteady Aerodynamic Solver," *The Aeronautical Journal*, Vol. 110, No. 1114, pp. 793-801, 2006.

[16] A. Castorrini, "Analysis of Helicopter Main Rotor Noise Prediction in Manoeuvring Flight," Master Thesis, University or Rome 'La Sapienza', 2013.

[17] B. Dang-Vu, P. Masarati, G. Quaranta, M. Gennaretti, M. Jump, I. Fuiorea, A. Ionita, Generic helicopter database, Technical Report Deliverable No. D3.1, EU funded project ARISTOTEL (GA no. 266073), 2011.

[18] D.H. Hodges, R.A. Ormiston, "Stability of Elastic Bending and Torsion of Uniform Cantilever Rotor Blades in Hover with Variable Structural Coupling," NASA TN D-8192, 1976.

[19] M. Gennaretti, L. Luceri, L. Morino, "A Unified Boundary Integral Methodology for Aerodynamics and Aeroacoustics of Rotors," *Journal of Sound and Vibration*, Vol. 200, No. 4, pp. 467-489, 1997.

[20] L. Morino, G. Bernardini, "Singularities in BIE's for the Laplace Equation; Joukowski Trailing-Edge Conjecture Revisited," *Journal of Engineering Analysis with Boundary Elements*, Vol. 25, pp. 805-818, 2001.

[21] G. Bernardini, J. Serafini, S. Ianniello, M. Gennaretti, "Aeroelastic Modeling Effect in Rotor BVI Noise Prediction," AIAA Paper 2006-2606, Proceedings of the 12th AIAA/CEAS Aeroacoustics Conference, Cambridge, Massachusets, USA, 2006.

[22] G. Bernardini, J. Serafini, S. Ianniello, M. Gennaretti, Assessment of Computational Models for the Effect of Aeroelasticity on BVI Noise Prediction, Int'l J. of Aeroacoustics 6 (3) (2007) 199-222.

A AEROELASTIC AND AERODYNAMIC MAIN ROTOR MODELLING

The simulation of the acoustic disturbance generated by rotors is a multidisciplinary task: blade aeroelasticity and aerodynamics accurate modelling are required to yield the blade surface pressure distribution that, in turn, is the input to an aeroacoustic tool providing the radiated noise. When significant blade-wake interaction effects occur, blade-wake miss distance may play a crucial role, and hence the evaluation of blade deformation and wake shape is essential[21,22]. The following sections provide a brief outline of the methodologies applied in this work to determine noise radiated by helicopter rotors.

A.1 Rotor Aeroelastic Modelling

Aeroelastic responses are obtained by combining a blade structural dynamics model with a three-dimensional, free-wake, aerodynamic formulation (see next section).

Blade structural dynamics is described through a beam-like model. It derives from a nonlinear, bending-torsion formulation valid for slender, homogeneous, isotropic, nonuniform, twisted blades, undergoing moderate displacements [10]. The radial displacement is eliminated from the set of equations by solving it in terms of local tension, and thus the resulting structural operator consists of a set of coupled nonlinear differential equations governing the bending of the elastic axis and the blade torsion [18].

The evaluation of the aerodynamic loads is obtained by a boundary element method for the solution of a boundary integral equation approach, suited for the analysis of potential flows around helicopter rotors in arbitrary flight condition [12] (see next section).

Coupling blade structural dynamics with aerodynamic loads yields an aeroelastic integro-partial differential system of equations. These are spatially integrated through the Galerkin approach, with the description of elastic axis deformation and cross-section torsion as linear combinations of shape functions satisfying homogeneous boundary conditions. This yields a set of nonlinear, ordinary differential equations of the type

$$\mathbf{M}(t)\ddot{\mathbf{q}} + \mathbf{C}(t)\dot{\mathbf{q}} + \mathbf{K}(t)\mathbf{q} = \mathbf{f}_{str}^{nl}(t,\mathbf{q}) + \mathbf{f}_{aer}(t,\mathbf{q}) \quad (3)$$

where $\mathbf{q}$ denotes the vector of the Lagrangian coordinates, $\mathbf{M}, \mathbf{C}$, and $\mathbf{K}$ are time-periodic, mass, damping, and stiffness structural matrices representing the linear structural terms. Non-linear structural contributions are collected in the forcing vector $\mathbf{f}_{str}^{nl}(t,\mathbf{q})$, whereas vector $\mathbf{f}_{aer}(t,\mathbf{q})$ collects the generalized aerodynamic forces.

The harmonic balance approach is applied to determine the periodic aeroelastic response during steady flight[13,14,15]. It is a methodology suitable for the analysis of the asymptotic solution (as time goes to infinity) of differential equations forced by periodic terms. Because of the presence of nonlinear contributions deriving from both structural terms and free-wake aerodynamics loads, the final system is solved using

an iterative approach, based on the Newton-Raphson method. On the other hand, non-periodic aeroelastic responses during unsteady helicopter maneuvers are evaluated through a time-marching solution algorithm based on a Newmark-β integration scheme.

A.2 Rotor Aerodynamic Solver

Considering incompressible, potential flows such that $\mathbf{v} = \nabla\varphi$, the rotor aerodynamics formulation applied assumes the potential field, φ, to be given by the superposition of an incident field, φ_I, and a scattered field, φ_S (*i.e.,* $\varphi = \varphi_I + \varphi_S$). The scattered potential is determined by sources and doublets distributions over the surfaces of the blades, S_B, and by doublets distributed over the wake portion that is very close to the trailing edge from which emanated (near wake, S_W^N). The incident potential field is associated to doublets distributed over the complementary wake region that compose the far wake S_W^F[12]. The wake surface partition is such that the far wake is the only wake portion that may come in contact with blades and generate BVI effects. The incident potential is discontinuous across S_W^F, whereas the scattered potential is discontinuous across S_W^N and is represented by[12]

$$\varphi_S(\mathbf{x},t) = \int_{S_B} \left[G\,(v_n - u_n) - \varphi_S \frac{\partial G}{\partial n} \right] \mathrm{d}S(\mathbf{y}) - \int_{S_W^N} \Delta\varphi_S \, \frac{\partial G}{\partial n} \, \mathrm{d}S(\mathbf{y}) \tag{4}$$

where $G = -1/4\pi\, r$ is the unit-source solution of the three-dimensional Laplace equation, with $r = \|\mathbf{y}-\mathbf{x}\|$, while $\Delta\varphi_S$ is the potential jump across the wake surface, known from past history of potential discontinuity at the blade trailing edge through the Kutta-Joukowski condition[19,20]. In addition, $v_n = \mathbf{v}_B \cdot \mathbf{n}$, with $\mathbf{v}_B$ representing the blade velocity and $\mathbf{n}$ its outward unit normal, whereas $u_n = \mathbf{u}_I \cdot \mathbf{n}$, with $\mathbf{u}_I$ denoting the velocity induced by the far wake.

Considering the far wake discretized into M panels, assuming the potential jump constant over each panel, and recalling the equivalence between surface distribution of doublets and vortices, the incident velocity field is evaluated through the Biot-Savart law applied to the vortices having the shape of the panel contours. In order to assure a regular distribution of the induced velocity within the vortex core, and thus a stable and regular solution even in blade-vortex impact conditions, a Rankine finite-thickness vortex model is introduced in the Biot-Savart law[12]. Wake-induced velocity field is applied to evaluate the term u_n in Eq. (4), as well as the velocity field from which the wake shape evolution is determined in a free-wake analysis. Note that, for an accurate prediction of BVI phenomena, the accurate evaluation of the wake distorted shape is essential in that a crucial role is played by the relative position between body and wake.

In this formulation, the incident potential affects the scattered potential through the induced-velocity, while the scattered potential affects the incident potential by its trailing-edge discontinuity that is convected along the wake and yields the intensity of the vortices of the far wake[12]. Once the potential field is known, the Bernoulli theorem yields the pressure distribution to be provided to aeroelastic and aeroacoustic solvers[14].